

# Anisoplanicity studies within NGC6871

Jason A. Marshall<sup>a</sup>, Mitchell Troy<sup>b</sup>, Richard Dekany<sup>b</sup>, Frank G. Dekens<sup>b</sup>

<sup>a</sup>Dept. of Physics & Astronomy, Univ. of California/Los Angeles

<sup>b</sup>Jet Propulsion Laboratory, California Institute of Technology, Pasadena, CA 91109

## ABSTRACT

Images corrected with adaptive optics benefit from an increase in the amount of flux contained within the diffraction-limited core. The degree of this correction is measured by the Strehl ratio, equal to the ratio of the maximum observed intensity to the maximum theoretical intensity. Natural guide star adaptive optics systems are limited by the need for a guide star of adequate magnitude within suitable proximity to the science target. Thus, the above-described benefit can only be obtained for objects over a fraction of the total sky. Two nights of imaging the central region of the open star cluster NGC6871 with the Palomar Adaptive Optics System has supplied measurements of the Strehl ratio for numerous stars within the field. These measurements were used to calculate K band isoplanatic angles of 39 arcseconds (UT 1999 May 31) and 50 arcseconds (UT 1999 August 1). These isoplanatic angles are compared to those derived from Kolmogorov atmospheric theory, and their implications for adaptive optics systems are discussed.

**Keywords:** Adaptive optics, atmospheric turbulence, anisoplanicity

## 1. INTRODUCTION

There are many papers describing the error terms that contribute to determine the performance of a natural guide star adaptive optics (AO) system<sup>1,3</sup>. In this paper, we will concentrate on the error term due to anisoplanatism. This effect occurs as a result of the different propagation paths through the atmosphere for non-coaxial guide star / target object systems. These varied paths produce slightly different wavefront distortions and therefore introduce an error term when one wavefront is used to correct for the other. In section two of this paper, we define the isoplanatic angle and provide its formulaic representations. This is followed in section three by the details of the observations of NGC6871, followed in section four by a description of the Strehl ratio measurement algorithm we developed. Section five details the Monte Carlo simulations we performed to measure the systematic and random errors in our Strehl ratio algorithm. In the final two sections, the results of this analysis, measurements of the isoplanatic angle for two seeing conditions, as well as its implications for adaptive optics and the Palomar Adaptive Optics System<sup>2</sup> (PALAO) will be discussed.

## 2. ANISOPLANATISM

A successful correction with an adaptive optics system requires that the science target be located in the vicinity of an adequately bright guide star. A brighter guide star results in a greater number of photons that reach the telescope, thus providing a higher signal-to-noise ratio (SNR) for wavefront sensor readings. For any wavefront sensor camera, this increased SNR reduces wavefront measurement uncertainties. Data concerning the relationship between the photometric properties of the guide star and the quality of the correction for PALAO can be found in Troy et al.<sup>2</sup>.

The isoplanatic angle defines the radius of a circle upon the sky within which atmospheric wavefront disturbances may be considered approximately uniform (see the definition of  $r_0$  below). This angle,  $\theta_0$ , is defined as<sup>1</sup>

$$\theta_0 = [2.914 k^2 (\sec \zeta)^{8/3} \int dh C_N^2(h) h^{5/3}]^{3/5}, \quad (1)$$

where  $\zeta$  is the zenith angle,  $k = 2\pi/\lambda$ , and  $C_N$  is the index of refraction structure function, as a function of height,  $h$ . We note that for PALAO, the deformable mirror is conjugate to the primary mirror ( $h = 0$ ). Thus, even with the AO system correcting the atmosphere, the integral in Equation (1) is unchanged and our quoted isoplanatic angles are true to this definition. Care should be taken however when quoting such a value for a system in which the deformable mirror is not conjugate to the primary mirror, as the values may differ. A practical approximation for the isoplanatic angle is given by<sup>3</sup>

$$\theta_0 = 0.314 r_0/h_0, \quad (2)$$

where  $r_0$  is the atmospheric coherence length, or Fried parameter<sup>4</sup>, and  $h_0$  is the weighted average height of the turbulence. A convenient approximation is that  $r_0$  is the radius of an aperture for which the RMS wavefront phase error is equal to 1 radian. The quality of the AO correction decreases as the guide star is displaced from the target object. This effect, known as anisoplanatism, occurs because the guide star wavefront is sampling a slightly different atmospheric wedge. As a result, the measured aberrations begin to apply less and less to the actual target object. In practice, this means that as the guide star is moved further from the axis of the target object, the obtainable Strehl ratio decreases. The form of this relationship, based upon Kolmogorov turbulence, is expressed by<sup>1</sup>

$$S(\theta) \propto e^{-(\theta/\theta_0)^{5/3}}, \quad (3)$$

where  $\theta$  is the angular distance to the target object from the guide star. The returned Strehl ratio will fall to approximately 37% of its on-axis value when the target object is displaced by one isoplanatic angle.

### 3. OBSERVATIONS

The Palomar Adaptive Optics System sits at the Cassegrain focus beneath the 200-inch Hale Telescope on Mount Palomar, California. The system operates in tandem with the Palomar High Angular Resolution Observer<sup>5</sup> (PHARO), a science camera designed and built at Cornell University. These instruments were used UT 1999 May 31 and UT 1999 August 1 to observe the central region of NGC6871 (20h 05m 56.4s, +35d 47m 13s), a young (2-7 Myr) open cluster / HII region at a distance of 1.9 kpc. Imaging was performed with the AO system operating at 500 Hz, locked on the  $V = 6.81$  central star SAO69402. The average K band seeing was  $\sim 1.1$  arcseconds on the first night and  $\sim 0.8$  arcseconds on the second.

During the first night, four images with integration times of one minute were taken through the K band (2.2  $\mu\text{m}$ ) near-IR filter. All imaging was performed with a 0.04 arcsecond plate scale; thus, the 1024x1024 pixel CCD provided a 41x41 arcsecond field of view. Sky background images were taken at three dither positions and a flat field was produced from a series of twilight flats taken the previous morning. Raw images were sky subtracted, flat-fielded, and known bad pixels were interpolated over. Finally, the individual integrations were shifted and median combined, giving a closed loop image with a total effective integration time of four minutes. This image is presented in Figure 1.

During the second night, twelve K band images, each with an integration time of twenty seconds, were reduced and combined as outlined above to produce a single image with an effective integration time of four minutes. This image is presented in Figure 2. Note the slight decrease in the size of the stellar cores, resulting from the improved seeing conditions, from the first to the second night. The six brightest stars in both images are saturated, and the ring shaped object on the right edge is an artifact ghost image resulting from a reflection within the AO system.

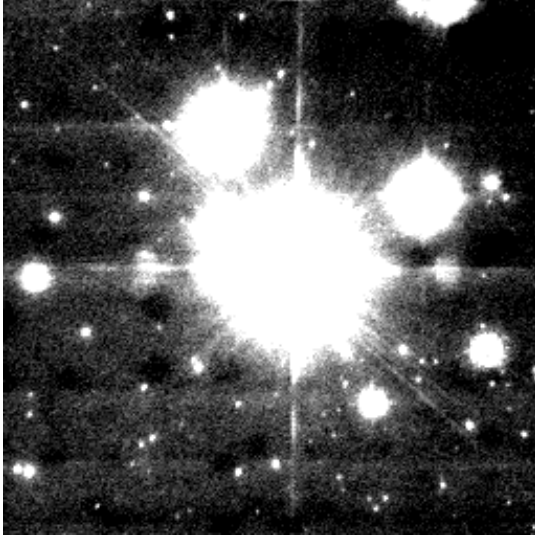


Figure 1. K band image of NGC6871 taken with the Palomar Adaptive Optics System and PHARO science camera on UT 1999 May 31. The average seeing on this night was 1.1 arcseconds.

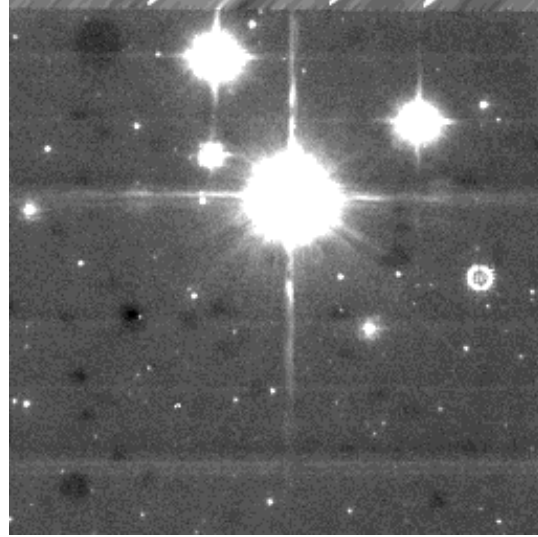


Figure 2. K band image of NGC6871 taken with the Palomar Adaptive Optics System and PHARO science camera on UT 1999 August 1. The average seeing on this night was 0.8 arcseconds.

#### 4. STREHL RATIO MEASUREMENT

Two metrics are commonly used to quantify the performance of an adaptive optics system. The first of these, the full-width-at-half-maximum (FWHM), provides a measure of the characteristic width of the point spread function (PSF). An effectively performing AO system will decrease this width, ideally to the diffraction-limit set by the dimensions of the telescope. As the width of the PSF decreases towards this diffraction-limit, an increasing percentage of the total flux from the observed object becomes concentrated within the central core of the image. The second metric, the Strehl ratio, is a measure of the degree to which this concentration of flux occurs. Specifically, the Strehl ratio is equal to the ratio of the maximum central intensity of the image to the maximum central intensity of a diffraction-limited image having identical integrated flux.

In this paper, the Strehl ratio will be used as the primary tool of analysis. To perform this study, we developed a package of IDL<sup>7</sup> programs designed to identify sources within an image, calculate their Strehl ratios, and perform a fit to this data to calculate the isoplanatic angle. The following is an outline of the algorithm we use to calculate Strehl ratios within a field of stars. We first create a theoretical diffraction-limited image with integrated intensity equal to unity for each object in the field, and position it at its measured centroid location. We then sum the total flux for each individual object from the observed CCD image and multiply the corresponding theoretical image by this value. This gives individual diffraction-limited images for each object, all having an integrated flux equal to its observed counterpart. The individual theoretical images are then added together to create one large diffraction-limited image, modeling the observed stellar field. The observed and theoretical peaks are determined for each object using IDL's bi-cubic interpolation routine at the centroid location of the appropriate image. The ratio of these two peaks provides a measure of the Strehl ratio.

While the idea is simple, a practical calculation of accurate Strehl ratios is difficult. The Strehl ratio algorithm is very sensitive to the accuracy of the flux measurements. This requires an accurate photometry algorithm with robust background estimation abilities. Another difficulty arises from the fact that the PSF is not constant across the field for images corrected with adaptive optics. Thus, one cannot simply rely upon a fixed aperture photometry algorithm using a single aperture radius. Our solution to these difficulties was to integrate E. Bertin's source extraction and photometry software package SExtractor<sup>6</sup> into our AO

analysis package. SExtractor offers four different photometric modes: isophotal, circular aperture, adaptive aperture, and corrected isophotal. This package was written to detect and perform photometric calculations upon galaxy fields. As such, many of these photometric modes allow for the possibility of a non-circularly symmetric source. This works out well for images corrected with adaptive optics, as the stellar PSF is not strictly circular. This effect becomes pronounced for objects situated far from the guide star, where the PSF often becomes elongated into an ellipse. We chose to use the adaptive aperture photometry mode offered by SExtractor. This routine, as described by Bertin & Arnouts<sup>6</sup>, uses the second order moments of the object profile to define an equivalent bivariate gaussian profile with mean standard deviation  $\sigma_{\text{iso}}$ . An elliptical aperture is defined from these moments and scaled to  $6 \cdot \sigma_{\text{iso}}$ , corresponding roughly to two isophotal radii. Finally, summed within this aperture, the value

$$r_1 = \Sigma r \cdot I(r) / \Sigma I(r) \quad (4)$$

is used to define an elliptical aperture with principal axes  $\epsilon k r_1$  and  $k r_1 / \epsilon$ , where  $\epsilon$  is the ellipticity. In this routine,  $k$  is set equal to 2.5, for which the mean fraction of flux loss is  $\sim 6\%$ . Using this method for each object individually, the aperture assigned is ideally suited to its unique PSF. This results in accurate aperture photometry, and therefore more accurate Strehl measurements across the field.

## 5. STREHL RATIO UNCERTAINTIES

We performed a series of Monte Carlo simulations to measure the absolute calibration errors and random uncertainties of our Strehl ratios. We created model objects of a specified Strehl ratio and SNR, inserted them at random locations into our observed fields, and measured the resulting Strehl ratios using the same techniques as used for objects in our observed fields. Model objects were created by superimposing two PSF's, a Gaussian halo and an Airy core, scaled by the appropriate factors to obtain an object of the desired Strehl ratio. In functional form, these objects were modeled as

$$I(x,y) = (1 - S) \cdot G(x,y) + (S) \cdot A(x,y), \quad (5)$$

where  $S$  is the Strehl ratio,  $G(x,y)$  is a Gaussian function with width set by the open-loop seeing, and  $A(x,y)$  is an Airy function. As the scale factor for the two PSF's is only approximate, we iterate upon the value of  $S$  until the ratio

$$I(x_0,y_0) / A(x_0,y_0), \quad (6)$$

where  $x_0$  and  $y_0$  are the centroid locations, is equal to the desired Strehl ratio within 0.01%. We perform this iterative process using a 0.005 arcsecond plate scale in order to prevent measurement errors of the peak object intensities resulting from insufficient sampling. The iterated value of  $S$  is then used to create the model object within an image of the desired pixel size. Inserting a number of these model objects into an image and measuring their Strehl ratios provides both the random errors in the measurement as well as a value for the systematic error present in our algorithm, the latter of which provides an absolute calibration for our measured Strehl ratios.

We first produced a K band image with a Strehl ratio of 1 and positioned it at random within a noiseless field. Using SExtractor's adaptive aperture photometry, we measured a Strehl ratio of 1 with an uncertainty of  $10^{-5}$ . For an object with a Strehl ratio of 0.05 in the same noiseless field, we measured a Strehl ratio of 0.049. Our error estimation algorithm returns a systematic uncertainty (defined as the difference of the modeled Strehl ratio from the measured Strehl ratio) of  $-0.001$  and a random uncertainty of  $10^{-5}$ . The slight systematic error is due to peak measurement errors caused by our 0.04 arcsecond plate scale. These tests show that the Strehl ratios reported by our algorithm are accurate for a noiseless image.

We next performed the same series of simulations using our observed images to measure the uncertainties in a field in which background noise is present. We first masked regions within three  $1 \cdot \sigma$  isophotal radii (defined as the contour along which the source flux is within  $1 \cdot \sigma$  of the background noise) of all detected

objects. We then found random coordinates outside of these masked regions, and measured the local background noise. This value was used to determine the required integrated intensity of the model object to obtain the desired signal-to-noise ratio. We calculated the SNR as

$$\text{SNR} = F_T / [F_T + N_p \sigma^2]^{1/2}, \quad (7)$$

where  $F_T$  is the total integrated flux,  $N_p$  is the number of pixels over which this flux was summed, and  $\sigma$  is the local RMS background noise. The results of these Monte Carlo simulations are plotted in Figure 3. The random and systematic errors, presented as a percentage of the Strehl ratio, are plotted as a function of SNR and input object Strehl ratio. Model objects for the SNR profile had a constant Strehl ratio of 0.4 while objects for the Strehl ratio profile had a constant SNR of 50.0. As the SNR and Strehl ratios increase, uncertainties in the flux and peak value measurements decrease. This causes the observed decrease in the random errors. The fall of the systematic errors can be partially attributed to this decrease in measurement uncertainties, although their full behavior is not yet completely understood.

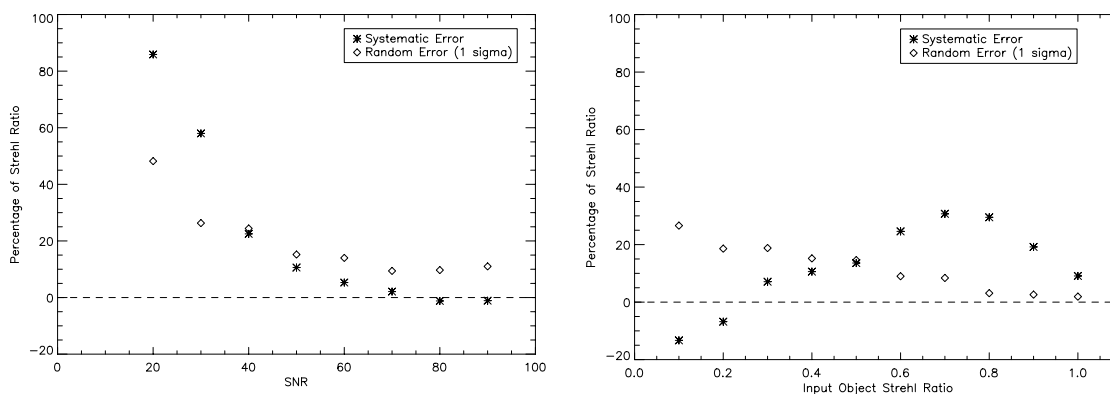


Figure 3. The random and systematic errors in our Strehl ratio calculation algorithm as determined by Monte Carlo simulations. These errors, derived from 20 simulated objects per bin, are plotted as a function of signal-to-noise ratio and input object Strehl ratio. The Strehl ratio of all objects in the SNR plot is 0.4 and the SNR of all objects in the input Strehl ratio plot is 50.0.

## 6. RESULTS

We ran our anisoplanicity analysis routine on both of the final combined K band images. In each of these images, the central star and several of its surrounding companions are saturated. As such, objects located within  $\sim 10$  arcseconds of the guide star were excluded from the SExtractor catalogue of detected sources. This decision was made in order to exclude both the saturated sources and any other sources that may have been in areas of high background contamination resulting from the saturated sources. We chose to restrict the SExtractor catalogue to well sampled objects, as we found that faint sources with low signal-to-noise ratios had large uncertainties (see Figure 3). We selected these sources by applying a minimum signal-to-noise ratio threshold. Objects in this analysis had signal-to-noise ratios ranging from 30 to 90. Errors were calculated by performing the above-described Monte Carlo simulation for each object, using its measured SNR and Strehl ratio as the input for the model objects. These simulations were performed using 20 model objects for each source.

Figure 4 displays the K band Strehl ratio of all analyzed objects as a function of their distance to the guide star for each of the two seeing conditions. In Figure 4, we have plotted Strehl ratios in two ways. The first, plotted as asterisks, represent the Strehl ratios uncorrected for the measured systematic errors. The second, plotted as diamonds, represent the corrected Strehl ratios. Figure 5 gives the FWHM of all analyzed sources as a function of their displacement from the guide star for each of the two nights.

The solid lines in Figure 4 represent the best fit of the corrected data to the model curve

$$S(\theta) = A_0 e^{-(\theta/\theta_0)^{5/3}}, \quad (8)$$

where  $A_0$  is the on-axis Strehl ratio,  $\theta$  is the guide star displacement, and as before,  $\theta_0$  is the isoplanatic angle. We used these fits to estimate the isoplanatic angles and on-axis Strehl ratios, as well as their uncertainties. The results of these fits are provided in Table 1.

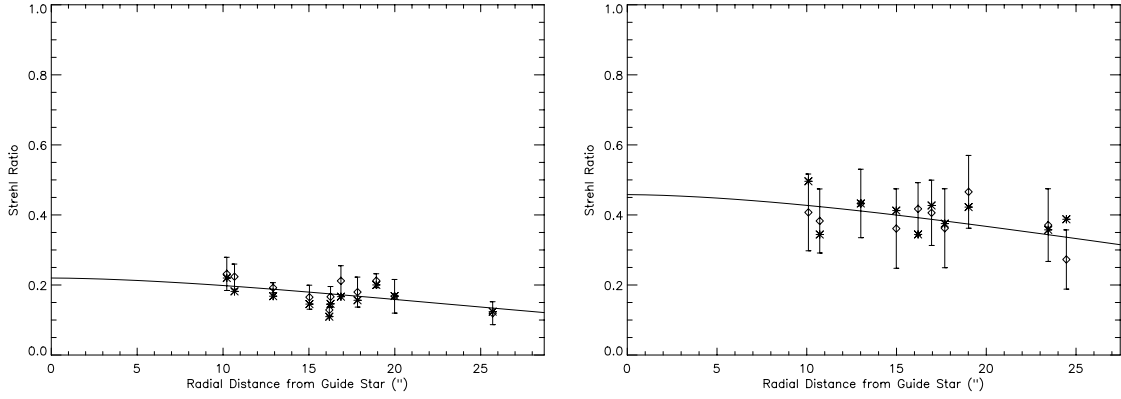


Figure 4. K band Strehl ratios as a function of guide star displacement. Data on the left is for 1.1 arcsecond K band seeing (UT 1999 May 31) while that on the right is for 0.8 arcsecond K band seeing (UT 1999 August 1). Diamonds represent the Strehl ratio corrected for systematic errors while asterisks represent the uncorrected values. The solid line is the fit of the corrected Strehl ratios to Equation (8).

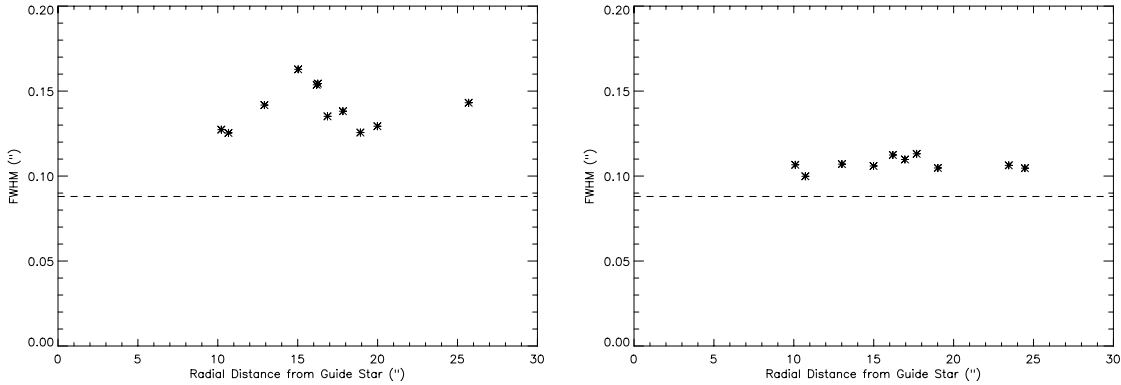


Figure 5. The FWHM of analyzed objects as a function of guide star displacement. Data on the left is for 1.1 arcsecond K band seeing (UT 1999 May 31) while that on the right is for 0.8 arcsecond K band seeing (UT 1999 August 1). The dashed line is the K band diffraction-limited FWHM of 0.088 arcseconds.

	<b>1.1" Seeing (UT 1999 May 31)</b>	<b>0.8" Seeing (UT 1999 August 1)</b>
<b>K</b>	$A_0 = 0.219 \pm 0.029$	$A_0 = 0.458 \pm 0.087$
	$\theta_0 = 39 \pm 13''$	$\theta_0 = 50 \pm 32''$

Table 1. Isoplanatic angle ( $\theta_0$ ) and on-axis Strehl ratio ( $A_0$ ) calculated from fitting data in Figure 4 with Equation (8).

The K band diffraction-limit of the 200-inch Palomar telescope using the PHARO camera is 0.088 arcseconds. K band seeing of 1.1 arcseconds (UT 1999 May 31) produced a mean FWHM of 0.14 arcseconds, the result of which was a fairly low on-axis Strehl ratio. On the second night of observing (UT 1999 August 1), 0.8 arcsecond seeing produced images with a mean FWHM of 0.11 arcseconds. This slight improvement in the FWHM resulted in much higher Strehl ratios. The FWHM from both nights are nearly constant across the field, although all are slightly greater than the K band diffraction-limit. This flat profile may indicate that the system was tip-tilt limited.

## 7. DISCUSSION / FUTURE WORK

For our observations, the guide star was positioned in the center of the field. This limited the angular separation of target objects to ~25 arcseconds. By positioning the guide star in one of the corners of the PHARO detector, one could obtain Strehl ratios for objects at an angular separation of nearly 60 arcseconds. This would alleviate one difficulty we encountered with our observations: for both nights, our isoplanatic angles were much larger than the maximum guide star / target object separation angle. This limited coverage introduced uncertainty into the fit. Thus, as observed in our data, a smaller isoplanatic angle has less uncertainty than a larger one.

Given a single measurement of the isoplanatic angle, we may use the relationship

$$\theta_0(\lambda) = \theta_0(\lambda_0)(\lambda/\lambda_0)^{6/5} \quad (9)$$

to estimate the isoplanatic angle at any wavelength. Here,  $\lambda_0$  is the reference wavelength and  $\lambda$  is the desired wavelength. For 0.8 arcsecond seeing, the K band isoplanatic angle of 50 arcseconds implies an isoplanatic angle of 34 arcseconds in H (1.6  $\mu\text{m}$ ), and 25 arcseconds in J (1.25  $\mu\text{m}$ ). For 1.1 arcsecond seeing, the K band isoplanatic angle of 39 arcseconds implies an isoplanatic angle of 27 arcseconds in H and 20 arcseconds in J.

The measured K band isoplanatic angles imply that scientifically useful observations could be made with guide star / target object angular separations well in excess of 50 arcseconds. With a maximum field of view of 41x41 arcseconds, this distance is greater than PALAO can currently effectively utilize. These results therefore suggest that it would be beneficial to develop techniques to acquire and lock on guide stars at angular distances beyond the capabilities of the current system.

Given an estimated value of  $r_0$ , Equation (2) allows us to calculate a value for the effective seeing height,  $h_0$ . For K band seeing of 0.8 arcseconds, we use  $\theta_0 = \lambda / r_0$  to estimate  $r_0 = 57$  cm. This, coupled with our stated value of  $\theta_0$ , provides an estimate for  $h_0$  of 738 meters. For K band seeing of 1.1 arcseconds,  $r_0$  is estimated to be 41 cm. This, along with an isoplanatic angle of 39 arcseconds provides an estimate for  $h_0$  of 681 meters. These values indicate that the dominant seeing layer resides at a low (< 1 km) altitude. This is important to the design of multi-conjugate AO systems, as the value of  $h_0$  determines the ideal location at which to place a deformable mirror conjugate to the effective seeing height.

The increasing interest in multi-conjugate adaptive optics systems emphasizes the need for methods to measure the altitude of the effective seeing layer. In the future, we would like to re-measure the isoplanatic angle to see if the quoted values of  $h_0$  are typical for Palomar. An improved estimate of  $r_0$  could be obtained through use of the AO telemetry data and the measurement of  $\theta_0$  could be improved using the technique described above. These changes, and an improved understanding of the systematic errors in our Strehl ratio calculations, will provide more accurate measurements and better statistics on the effective seeing layer height.

## ACKNOWLEDGMENTS

The work presented in this paper was carried out as part of the Summer Undergraduate Research Fellowship program at the California Institute of Technology, to whom our gratitude is extended.

## REFERENCES

1. D. G. Sandler, S. Stahl, J. R. P. Angel, M. Lloyd-Hart, D. McCarthy, "Adaptive Optics for Diffraction-Limited Infrared Imaging with 8 m Telescopes," *J. Opt. Soc. Am.* **A 11(2)**, pp. 925-945, 1994.
2. M. Troy, R. Dekany, G. Brack, F. Shi, B. Oppenheimer, T. Trinh, E. Bloemhof, T. Hayward, B. Brandl, F. Dekens, "Palomar adaptive optics project: status and performance," *SPIE Proceedings* **4007**, 2000.
3. J. M. Beckers, "Adaptive Optics For Astronomy: Principles, Performance and Applications," *Annual Reviews of Astronomy and Astrophysics* **31**, 1993.
4. D. L. Fried, "Statistics of a Geometrical Representation of Wavefront Distortion," *J. Opt. Soc. Am.* **55(11)**, pp. 1427-1435, 1965.
5. B. Brandl, T. Hayward, J. Houck, "PHARO (Palomar High Angular Resolution Observer): a dedicated NIR camera for the Palomar adaptive optics system," *SPIE Proceedings*, **3126**, 1997.
6. E. Bertin, S. Arnouts, "SExtractor: software for source extraction," *Astronomy and Astrophysics* **117**, 1996.
7. Interactive Data Language (IDL), Research Systems, Inc.